

## HIGHLY BIREFRINGENT FOUR-HOLE FIBER FOR PRESSURE SENSING

D. Chen

Institute of Information Optics  
Zhejiang Normal University  
Jinhua 321004, China

M.-L. V. Tse, C. Wu, H. Y. Fu, and H. Y. Tam

Photonics Research Centre  
Department of Electrical Engineering  
The Hong Kong Polytechnic University  
Hung Hom, Kowloon, Hong Kong SAR, China

**Abstract**—A highly birefringent four-hole fiber (FHF) with a pair of large air holes and a pair of small air holes are proposed for air/hydrostatic pressure sensing. The birefringence of the FHF can be up to 0.01 due to the rectangle-like fiber core surrounded by four air holes. Therefore, a FHF with a length of only several centimeters is required for high-sensitivity pressure sensing based on a Sagnac interferometer. Optical properties of the FHF such as effective index and birefringence are investigated. Pressure sensor based on the FHF depends on the pressure-induced refractive index change or pressure-induced birefringence. The stress distribution of the FHF subjected to an air/hydrostatic pressure is represented. Simulations show that the principal stress component parallel to the slow axis of the of the FHF under the air/hydrostatic pressure is greatly enhanced due to the existence of two large air holes, which consequently results in a high sensitivity of the FHF-based pressure sensor. Relationships between the pressure-induced birefringence and the radius of the large air hole, the external diameter of the FHF, or the ellipticity of the elliptical FHF are investigated. The polarimetric pressure sensitivity of the FHF can be up to 607 rad/MPa/m.

## 1. INTRODUCTION

Pressure sensors based on optical fibers have attracted considerable attentions for several decades due to their advantages such as small size, fiber compatibility, and immunity to electromagnetic interference. Early in 1979, Budiansky et al. discussed the pressure sensitivity of a clad optical fiber [1]. Later several pressure sensors based on birefringent fibers were reported [2–7]. To further improve the performance of the optical fiber based pressure sensors, significant efforts have been made to design suitable optical fibers. Side-hole fibers were proposed and demonstrated for pressure sensing [8–12]. More recently, several microstructured fibers (MSFs) (i.e., photonic crystal fibers (PCFs)) were also proposed for pressure sensing [13–22]. Thanks to the design flexibility of the cross-section, MSFs have achieved excellent properties in birefringence [23–29], dispersion [30–34], single polarization single mode [35–37], nonlinearity [38], and effective mode area [39–41] over the past several years. MSFs have shown some advantages for applications in optical fiber sensors, such as temperature insensitivity for strain sensing, high sensitivity for pressure sensing and so on. Compared with conventional single mode fiber (SMF), MSF is superior in acting as a stress-optic component.

In this paper, we propose a highly birefringent four-hole fiber (FHF) with a birefringence up to 0.01. By utilizing the physical property of the air-glass structure, the FHF can be used as an air/hydrostatic pressure sensor element offering high sensitivity. In our design, two large air holes and two small air holes are employed to form a rectangle-like fiber core which ensures the high birefringence of the FHF. The two large air holes have a high hole-size to fiber-size ratio, thus the pressure sensitivity is enhanced.

## 2. FIBER STRUCTURE AND PRINCIPLE

Figure 1 shows the cross-section of the proposed FHF with an external diameter ( $D$ ). A pair of large air holes with a radius ( $R$ ) is employed in the cross-section. The edge-to-edge distance between the two large air holes ( $L$ ) can be viewed as the width of the rectangle-like fiber core in the horizontal direction. The pair of small air holes with diameter ( $d$ ) ensures the confinement of the light propagating in the fiber core. The center-to-center distance between the two small air holes is  $H$ . The width of the rectangle-like fiber core can be viewed as  $H-d$ . To simplify analysis, the refractive indices of the pure silica and air are assumed to be 1.444 and 1, respectively. A full-vector finite-element method (FEM) [42] is used to investigate guided modes of the proposed FHF.

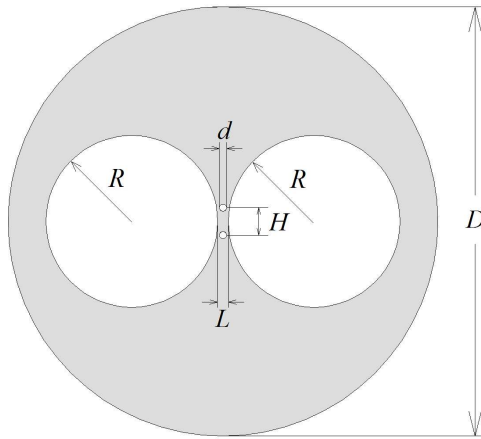


**Figure 1.** Cross-section of the FHF.

Due to the rectangle-like structure of the fiber core of the FHF, there are two fundamental modes with two orthogonal degenerated polarizations and two different effective indices. The phase modal birefringence of the optical fiber is defined as

$$B = n_{eff}^y - n_{eff}^x, \tag{1}$$

where  $n_{eff}^x$  and  $n_{eff}^y$  are the effective indices of the  $x$ -polarized mode and  $y$ -polarized mode of the optical fiber, respectively. When the FHF is subjected to an air/hydrostatic pressure, the stress induced by the pressure will result in refractive index change due to the photoelastic effect. The refractive index of the pure silica subjected to the pressure is given by [43]

$$\begin{aligned} n_x &= n_0 - C_1\sigma_x - C_2(\sigma_y + \sigma_z) \\ n_y &= n_0 - C_1\sigma_y - C_2(\sigma_x + \sigma_z) \end{aligned} \tag{2}$$

where  $\sigma_x$ ,  $\sigma_y$  and  $\sigma_z$  are the stress components,  $C_1 = 6.5 \times 10^{-13} \text{ m}^2/\text{N}$  and  $C_2 = 4.2 \times 10^{-13} \text{ m}^2/\text{N}$  are the stress-optic coefficients of pure silica. The pressure-induced index change is

$$\begin{aligned} \delta n_x &= n_x - n_0 = -C_1\sigma_x - C_2(\sigma_y + \sigma_z) \\ \delta n_y &= n_y - n_0 = -C_1\sigma_y - C_2(\sigma_x + \sigma_z) \end{aligned} \tag{3}$$

and the pressure-induced birefringence is

$$\delta B = n_y - n_x = (C_2 - C_1)(\sigma_x - \sigma_y) \tag{4}$$

An important parameter of the MSF for pressure sensing is the polarimetric pressure sensitivity, which is defined as

$$K_p = \frac{2\pi}{\lambda} \frac{dB}{dP} \quad (5)$$

where  $\lambda$ ,  $dP$ , and  $dB$  are the operation wavelength, pressure change and pressure-induced birefringence, respectively. We also use the FEM to calculate the stress distribution in the FHF under pressure. Note that the Young's modulus  $E_{\text{SiO}_2} = 73.1$  GPa and Poisson's ratio  $\nu_{\text{SiO}_2} = 0.17$  for the pure silica are used in our calculations.

The mechanism of the optical fiber pressure sensor is mainly based on two principles. The first one is the detection of the pressure-induced effective index change ( $\Delta n_{\text{eff}}$ ), e.g., by measuring the central wavelength shift ( $\Delta\lambda_B = \lambda \times \Delta n_{\text{eff}}/n_{\text{eff}}$ ) of a fiber Bragg grating (FBG) written in the pressure sensing fiber [43] (which needs an FBG written on the sensing fiber). The second one is the detection of the pressure-induced birefringence ( $\Delta B$ ), e.g., by measuring the pressure-induced wavelength shift ( $\Delta\lambda_p = \lambda \times \Delta B/B$ ) of the transmission spectrum of the pressure sensing fiber based on a Sagnac interferometer [19]. The latter method yields a higher sensitivity for pressure sensing if  $\Delta n_{\text{eff}} \approx \Delta B$ , since  $n_{\text{eff}} \gg B$  in an optical fiber. Thus, the proposed highly birefringent FHF is designed for pressure sensing based on a Sagnac interferometer demodulation.

### 3. PROPERTIES OF FOUR-HOLE FIBER

Optical properties such as the effective index, the birefringence and the confinement loss are very important for fiber-based pressure sensing. A FHF with parameters of  $L = 2 \mu\text{m}$ ,  $d = 2 \mu\text{m}$ ,  $H = 8 \mu\text{m}$ ,  $R = 25 \mu\text{m}$  and  $D = 125 \mu\text{m}$  is firstly investigated. Fig. 2(a) shows the effective index of the  $x$ -polarized (red curve with hollow circles) and  $y$ -polarized (black curve with hollow triangles) fundamental modes of the FHF. The effective index of the  $y$ -polarized fundamental mode is larger than that of the  $x$ -polarized fundamental mode. The large gap between the two index curves indicates a high birefringence of the FHF. Insets of Fig. 2(a) show the mode profiles (power flow) of the  $x$ -polarized (left inset) and  $y$ -polarized (right inset) fundamental modes of the FHF at the wavelength of 1550 nm and the corresponding confinement loss are 0.136 dB/m and 0.063 dB/m, respectively. Fig. 2(b) shows birefringence of the FHFs with parameters of ( $L = 2 \mu\text{m}$ ,  $d = 2 \mu\text{m}$ ,  $H = 8 \mu\text{m}$ ,  $R = 25 \mu\text{m}$ ,  $D = 125 \mu\text{m}$ ), ( $L = 2 \mu\text{m}$ ,  $d = 2 \mu\text{m}$ ,  $H = 8 \mu\text{m}$ ,  $R = 20 \mu\text{m}$ ,  $D = 125 \mu\text{m}$ ), ( $L = 3 \mu\text{m}$ ,  $d = 2 \mu\text{m}$ ,  $H = 8 \mu\text{m}$ ,  $R = 25 \mu\text{m}$ ,  $D = 125 \mu\text{m}$ ), and ( $L = 3 \mu\text{m}$ ,  $d = 2 \mu\text{m}$ ,  $H = 6 \mu\text{m}$ ,  $R = 25 \mu\text{m}$ ,  $D = 125 \mu\text{m}$ ). The birefringence of the FHF

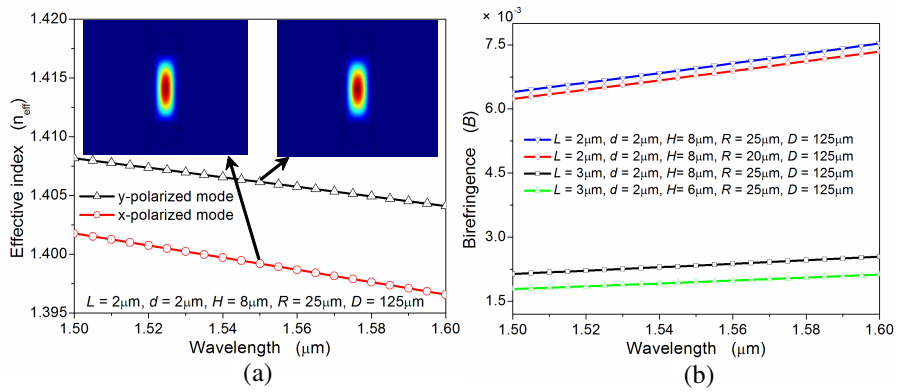


**Figure 2.** (a) Effective index of the  $x/y$ -polarized fundamental modes of the FHF. (b) Birefringence of the FHFs with different parameters. Insets of Fig. 2(a) show mode profiles (power flow) of the  $x/y$ -polarized fundamental modes of the FHF at the wavelength of 1550 nm.

with parameters of ( $L = 2 \mu\text{m}, d = 2 \mu\text{m}, H = 8 \mu\text{m}, R = 25 \mu\text{m}, D = 125 \mu\text{m}$ ) is about 0.007 at 1550 nm, which is almost 10 times of that of the recently reported polarization-maintaining photonic crystal fiber (PM-PCF) (used as a pressure sensor with a fiber length of several tens of centimeters) [19]. Thus, a segment of the proposed FHF with a length of several centimeters is enough for pressure sensing application (according to the Equation (3) in [19]). The simulation results in Fig. 2(b) show that the birefringence of the FHF mainly depends on parameters of the edge-to-edge distance ( $L$ ) of the two large air holes and the center-to-center distance ( $H$ ) between the two small air holes. The birefringence of the FHF can be up to 0.01 when  $L$  is less than  $2 \mu\text{m}$ . The radius ( $R$ ) of the large air hole does not play an important role in the birefringence of the FHF. In Fig. 2(b), one can see little difference of the birefringence for the two FHFs with different large air hole radius,  $R = 25 \mu\text{m}$  and  $R = 20 \mu\text{m}$ .

Above calculated results have shown that the proposed FHF have suitable optical properties such as the effective index, birefringence and confinement loss for the pressure sensing application, which ensure an guiding mode, a length at the order of centimeters, and an acceptable confinement loss at the order of 0.1 dB for the FHF. Next, we investigated the property of the FHF when it is under an air/hydrostatic pressure. We calculated the stress distribution of a FHF with the parameters of  $L = 2 \mu\text{m}, d = 2 \mu\text{m}, H = 8 \mu\text{m}, R = 25 \mu\text{m},$  and  $D = 125 \mu\text{m},$  with an air/hydrostatic pressure of

$P = 1$  MPa. Note that only radial stress components are considered in our calculations since the stress component  $\sigma_z$  is much smaller compared to  $\sigma_x$  or  $\sigma_y$ . Fig. 3 shows distributions of the principal stress component parallel to  $x$  axis of the structure ( $\sigma_x$ ) and the principal stress component parallel to  $y$  axis of the structure ( $\sigma_y$ ) in the cross-section of the FHF under an air/hydrostatic pressure of 1 MPa. The sub figures on the top of Fig. 3 show the  $\sigma_x$  and  $\sigma_y$  distribution of a quarter of the fiber cross-section. Figs. 3(a) and 3(b) show the  $\sigma_x$  and  $\sigma_y$  distributions along the  $x$  and  $y$  radial direction in the cross-section of the FHF. Compared to a solid SMF with an equivalent core size, the difference between  $\sigma_x$  and  $\sigma_y$  are much larger for the FHF. Particularly when we focus on the center of the fiber core, the values of  $\sigma_x$  and  $\sigma_y$  are  $-0.37$  MPa and  $-13.9$  MPa, and the corresponding pressure-induced index changes are  $\delta n_x = 5.86 \times 10^{-5}$  and  $\delta n_y = 1.06 \times 10^{-5}$ , respectively. Thus, we can calculate the pressure-induced birefringence which is  $\delta B = 4.8 \times 10^{-5}$  for the FHF with the parameters of  $L = 2 \mu\text{m}$ ,  $d = 2 \mu\text{m}$ ,  $H = 8 \mu\text{m}$ ,  $R = 25 \mu\text{m}$ , and  $D = 125 \mu\text{m}$  (when the pressure is 1 MPa). The polarimetric pressure sensitivity of the FHF

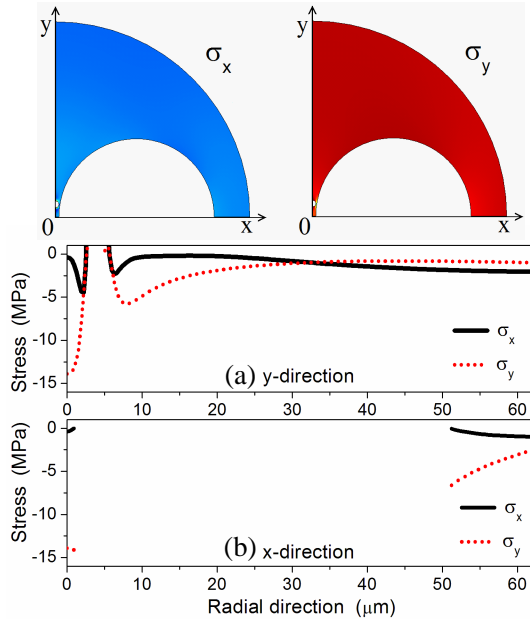


**Figure 3.** Distribution of the principal stress component ( $\sigma_x$ ) and the principal stress component ( $\sigma_y$ ) in the cross-section of the FHF under an air/hydrostatic pressure of 1 MPa.

is  $K_p = 195 \text{ rad/MPa/m}$ , which is more than 4 times of that recently reported in [22]. Note that the value of  $\sigma_y$  in the fiber core is almost 14 times of the value of the pressure utilized on the surface of the fiber cladding. This is mainly due to the existence and the arrangement of the large air holes in the cross-section of the FHF.

Figure 4(a) shows the linear relationship between the pressure-induced birefringence and the pressure for three FHF's with parameters of ( $L = 2 \mu\text{m}$ ,  $H = 8 \mu\text{m}$ ,  $d = 2 \mu\text{m}$ ,  $R = 25 \mu\text{m}$ , and  $D = 125 \mu\text{m}$ ), ( $L = 3 \mu\text{m}$ ,  $H = 8 \mu\text{m}$ ,  $d = 2 \mu\text{m}$ ,  $R = 25 \mu\text{m}$ , and  $D = 125 \mu\text{m}$ ), and ( $L = 3 \mu\text{m}$ ,  $H = 6 \mu\text{m}$ ,  $d = 2 \mu\text{m}$ ,  $R = 25 \mu\text{m}$ , and  $D = 125 \mu\text{m}$ ). The smaller edge-to-edge distance between the two large air holes ( $L$ ) and the larger center-to-center distance between the two small air holes ( $H$ ) will result in a higher polarimetric pressure sensitivity of the FHF. Fig. 4(b) shows the pressure-induced birefringence vs radius ( $R$ ) of two large air holes for three FHF's with parameters of ( $L = 2 \mu\text{m}$ ,  $H = 8 \mu\text{m}$ ,  $d = 2 \mu\text{m}$ , and  $D = 125 \mu\text{m}$ ), ( $L = 3 \mu\text{m}$ ,  $H = 8 \mu\text{m}$ ,  $d = 2 \mu\text{m}$ , and  $D = 125 \mu\text{m}$ ), and ( $L = 3 \mu\text{m}$ ,  $H = 6 \mu\text{m}$ ,  $d = 2 \mu\text{m}$ , and  $D = 125 \mu\text{m}$ ). Evidently the pressure-induced birefringence increases with the radius of large air holes. As mentioned above, the existence of the two large air holes in the cross-section of the FHF results in the large stress component  $\sigma_y$  in the fiber core region. For a better understanding, inset of Fig. 4(b) shows half of the cross-section of the FHF under the air/hydrostatic pressure. The  $y$ -direction pressure

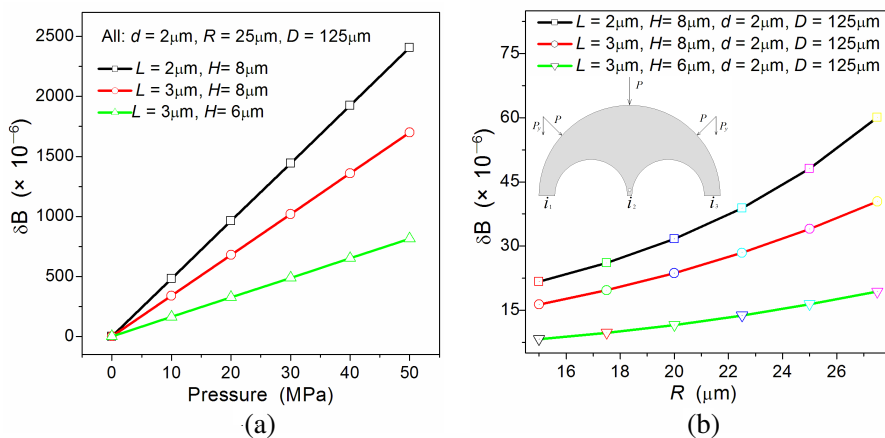


**Figure 4.** Pressure-induced birefringence vs (a) pressure and (b) radius ( $R$ ) of two large air holes for three FHF's with different structures. Inset of Fig. 4(b) shows half of the cross-section of the FHF under the air/hydrostatic pressure.

exerted on the surface of the fiber cladding is transmitted to three struts of the structure ( $i_1$ ,  $i_2$  and  $i_3$ ). When the external diameter of the FHF is fixed to  $D = 125 \mu\text{m}$ , the increasing radius of the large air hole means a smaller value of  $i_1 + i_2 + i_3$  (i.e., thinner struts) which results in a larger stress component  $\sigma_y$  when the air/hydrostatic pressure is a constant.

The relationship between the pressure-induced birefringence and the external diameter of the FHF is presented in Fig. 5. Note that, the size of the large air holes ( $R$ ) is varied with external diameter to keep size of there struts  $i_1$ ,  $i_2$ , and  $i_3$  unchanged, and the other parameters are fixed ( $L = 2 \mu\text{m}$ ,  $H = 8 \mu\text{m}$ , and  $d = 2 \mu\text{m}$ ). Fig. 5 shows that the relationship is linear. FHF with a larger external diameter relative to the core size can achieve larger pressure-induced birefringence (up to the order of  $10^{-4} \text{MPa}^{-1}$ ). The recently reported PM-PCF used as a pressure sensor [19] has a birefringence-pressure coefficient of about  $1.7 \times 10^{-6} \text{MPa}^{-1}$ , corresponding to a resolution of about 2.9 kPa. Thus, utilizing the FHF can achieve a resolution of several tens of Pa if the same setup is used. The polarimetric pressure sensitivity of the FHF with parameters of  $L = 2 \mu\text{m}$ ,  $d = 2 \mu\text{m}$ ,  $H = 8 \mu\text{m}$ ,  $R = 71.25 \mu\text{m}$ ,  $D = 300 \mu\text{m}$  is  $K_p = 607 \text{rad/MPa/m}$ , which is more than 14 times of that for the recently reported MSF [22].

Moreover, an elliptical FHF with a larger ellipticity (defined as  $D_x/D_y$ , shown in the inset of Fig. 6) can also achieve a higher pressure-induced birefringence. Fig. 6 shows the pressure-induced birefringence vs ellipticity ( $D_x/D_y$ ) of the FHFs with parameters of ( $R = 27.5 \mu\text{m}$ ,

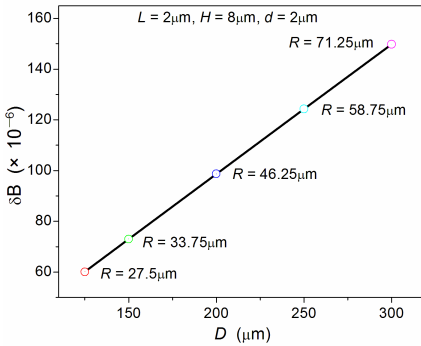


**Figure 5.** Pressure-induced birefringence vs external diameter ( $D$ ) of FHFs.

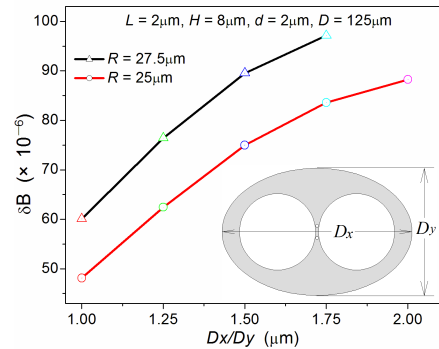


**Figure 6.** Pressure-induced birefringence vs ellipticity ( $D_x/D_y$ ) of FHFs. Inset shows the cross-section of the elliptical FHF.

$L = 2 \mu\text{m}$ ,  $H = 8 \mu\text{m}$ ,  $d = 2 \mu\text{m}$ , and  $D = D_x = 125 \mu\text{m}$ ), and ( $R = 25 \mu\text{m}$ ,  $L = 2 \mu\text{m}$ ,  $H = 8 \mu\text{m}$ ,  $d = 2 \mu\text{m}$ , and  $D = D_x = 125 \mu\text{m}$ ). The pressure-induced birefringence becomes higher when the ellipticity ( $D_x/D_y$ ) of the FHF increases. By considering the inset of Fig. 4(b), one can see that an elliptical FHF with a larger ellipticity will increase the  $y$ -direction (pressure-induced) force exerted on the surface, which consequently results in a larger stress component  $\sigma_y$  and also the larger pressure-induced birefringence.

#### 4. DISCUSSION AND CONCLUSION

Unlike the MSF with complex cross-section, the simple four air holes in the FHF can form a fiber core with expected optical properties such as high birefringence, which indicates that the FHF with a length of just several centimeters is sufficient for high-sensitivity pressure sensing based on a Sagnac interferometer. The FHF provides a structure to enhance the pressure sensitivity due to the existence of two large air holes. Our investigations in this paper have evidently pointed out three directions to further enhance the pressure sensitivity of the FHF. The first one is to use two larger air holes and a fiber core with smaller width between the holes. The second one is to use a FHF with a larger external diameter. The third one is to use an elliptical FHF with a larger ellipticity, which means a smaller diameter in the  $y$  direction (see inset of Fig. 6). However, for the practical application of a pressure sensor based on the FHF, the mechanical stability and the fabrication of the FHF should be considered. In addition, the pure silica FHF has the advantage of low temperature influence, which has been addressed in recent paper [21]. Regarding to the fabrication feasibility of the FHF with different size air holes in the cross-section, it is with high possibility to fabricate the FHF using the current fabrication techniques available when different air pressure in the large air hole and small air hole is well controlled and the silica tube for two kinds of air holes are well fixed during the fiber drawing processing. Please note that there are several MSFs with different size air holes in the cross-section have been fabricated [16–19].

In conclusion, we have proposed a highly birefringent FHF with a rectangle-like fiber core surrounded by a pair of large air holes and two very small air holes. Effective index and birefringence of the FHF with different parameters in the 1.5 micrometer region is investigated. The birefringence of the FHF is up to 0.01 due to the rectangle-like fiber core surrounded by the four air holes. The stress distribution of the FHF under the air/hydrostatic pressure has been presented. Simulations show that the principal stress component parallel to the

slow axis of the FHF under hydrostatic pressure is greatly enhanced due to the existence of the two large air holes, which consequently results in high sensitivity of pressure sensing based on the FHF. The relationships between the pressure-induced birefringence change and the radius of the large air hole, the external diameter of the FHF, or the ellipticity of the elliptical FHF are investigated. Simulation results have shown that the polarimetric pressure sensitivity of a FHF with outer diameter of 300  $\mu\text{m}$  can be up to 607 rad/MPa/m, which is more than 14 times of that for the recently reported MSF.

## ACKNOWLEDGMENT

This work is supported by the Natural Science Foundation of China under project (No. 61007029) and the Central Research Grant of The Hong Kong Polytechnic University under the Postdoctoral Fellowship (Project No. G-YX2D).

## REFERENCES

1. Budiansky, B., D. C. Drucker, G. S. Kino, and J. R. Rice, "Pressure sensitivity of a clad optical fiber," *Appl. Opt.*, Vol. 18, 4085–4088, 1979.
2. Bock, W. J. and A. W. Domanski, "High hydrostatic pressure effects in highly birefringent optical fibers," *J. Lightwave Technol.*, Vol. 7, 1279–1283, 1989.
3. Chiang, K. S. and D. Wong, "Hydrostatic pressure induced birefringence in a highly birefringent optical fiber," *Electron. Lett.*, Vol. 26, 1952–1954, 1990.
4. Chiang, K. S., "Pressure-induced birefringence in a coated highly birefringent optical fiber," *J. Lightwave Technol.*, Vol. 8, 1850–1855, 1990.
5. Wang, A., S. He, X. Fang, X. Jin, and J. Lin, "Optical fiber pressure sensor based on photoelasticity and its application," *J. Lightwave Technol.*, Vol. 10, 1466–1472, 1992.
6. Wolinski, T. R. and W. J. Bock, "Birefringence measurement under hydrostatic pressure in twisted highly birefringent fibers," *IEEE Trans. Instrum. Meas.*, Vol. 44, 708–711, 1995.
7. Ma, J., W. Tang, and W. Zhou, "Optical-fiber sensor for simultaneous measurement of pressure and temperature: Analysis of cross sensitivity," *Appl. Opt.*, Vol. 35, 5206–5210, 1996.
8. Charasse, M. N., M. Turpin, and J. P. Le Pesant, "Dynamic

- pressure sensing with a side-hole birefringent optical fiber,” *Opt. Lett.*, Vol. 16, 1043–1045, 1991.
9. Clowes, J. R., S. Syngellakis, and M. N. Zervas, “Pressure sensitivity of side-hole optical fiber sensors,” *IEEE Photon. Technol. Lett.*, Vol. 10, 857–859, 1998.
  10. Zhao, Y. and F. Ansari, “Intrinsic single-mode fiber-optic pressure sensor,” *IEEE Photon. Technol. Lett.*, Vol. 13, 1212–1214, 2001.
  11. Nawrocka, M. S., W. J. Bock, and W. Urbanczyk, “Dynamic high-pressure calibration of the fiber-optic sensor based on birefringent side-hole fibers,” *J. Sens.*, Vol. 5, 1011–1018, 2005.
  12. Frazao, O., S. O. Silva, J. M. Baptista, J. L. Santos, G. Statkiewicz-Barabach, W. Urbanczyk, and J. Wojcik, “Simultaneous measurement of multiparameters using a Sagnac interferometer with polarization maintaining side-hole fiber,” *Appl. Opt.*, Vol. 47, 4841–4848, 2008.
  13. Statkiewicz, G., T. Martynkien, and W. Urbanczyk, “Measurements of modal birefringence and polarimetric sensitivity of the birefringent holey fiber to hydrostatic pressure and strain,” *Opt. Communications*, Vol. 241, 339–348, 2004.
  14. Szpulak, M., T. Martynkien, and W. Urbanczyk, “Effects of hydrostatic pressure on phase and group modal birefringence in microstructured holey fibers,” *Appl. Opt.*, Vol. 43, 4739–4744, 2004.
  15. MacPherson, W. N., E. J. Rigg, J. D. C. Jones, V. V. Ravi Kanth Kumar, J. C. Knight, and P. St. J. Russell, “Finite-element analysis and experimental results for a microstructured fiber with enhanced hydrostatic pressure sensitivity,” *J. Lightwave Technol.*, Vol. 23, 1227–1231, 2005.
  16. Bock, W. J., J. Chen, and W. Urbanczyk, “A photonic crystal fiber sensor for pressure measurement,” *IEEE Trans. Instrum. Meas.*, Vol. 55, 1119–1123, 2006.
  17. Martynkien, T., G. Statkiewicz, M. Szpulak, J. Olszewski, G. Golojuch, W. Urbanczyk, J. Wojcik, P. Mergo, M. Makara, T. Nasilowski, F. Berghmans, and H. Thienpont, “Measurements of polarimetric sensitivity to temperature in birefringent holey fibres,” *Meas. Sci. Technol.*, Vol. 18, 3055–3060, 2007.
  18. Shinde, Y. S. and H. K. Gahir, “Dynamic pressure sensing study using photonic crystal fiber: application to tsunami sensing,” *IEEE Photon. Technol. Lett.*, Vol. 20, 279–281, 2008.
  19. Fu, H. Y., H. Y. Tam, L. Y. Shao, X. Dong, P. K. A. Wai, C. Lu,

- and S. K. Khijwania, "Pressure sensor realized with polarization-maintaining photonic crystal fiber-based Sagnac interferometer," *Appl. Opt.*, Vol. 47, 2835–2839, 2008.
20. Oliveira, R. E. P. de, C. J. S. de Matos, J. G. Hayashi, and C. M. B. Cordeiro, "Pressure sensing based on nonconventional air-guiding transmission windows in hollow-core photonic crystal fibers," *J. Lightwave Technol.*, Vol. 27, 1605–1609, 2009.
  21. Szczurowski, M. K., T. Martynkien, G. Statkiewicz-Barabach, W. Urbanczyk, and D. J. Webb, "Measurements of polarimetric sensitivity to hydrostatic pressure, strain and temperature in birefringent dual-core microstructured polymer fiber," *Opt. Express*, Vol. 18, 12076–12087, 2010.
  22. Martynkien, T., G. Statkiewicz-Barabach, J. Olszewski, J. Wojcik, P. Mergo, T. Geernaert, C. Sonnenfeld, A. Anuszkiewicz, M. K. Szczurowski, K. Tarnowski, M. Makara, K. Skorupski, J. Klimek, K. Poturaj, W. Urbanczyk, T. Nasilowski, F. Berghmans, and H. Thienpont, "Highly birefringent microstructured fibers with enhanced sensitivity to hydrostatic pressure," *Opt. Express*, Vol. 18, 15113–15121, 2010.
  23. Ortigosa-Blanch, A., J. C. Knight, W. J. Wadsworth, J. Arriaga, B. J. Mangan, T. A. Birks, and P. St. J. Russel, "Highly birefringent photonic crystal fibers," *Opt. Lett.*, Vol. 25, 1325–1327, 2000.
  24. Chau, Y.-F., H.-H. Yeh, and D. P. Tsai, "Significantly enhanced birefringence of photonic crystal fiber using rotational binary unit cell in fiber cladding," *Jpn. J. Appl. Phys.*, Vol. 46, 1048–1051, 2007.
  25. Chen, D. and L. Shen, "Ultra-high birefringent photonic crystal fiber with ultralow confinement loss," *IEEE Photon. Technol. Lett.*, Vol. 19, 185–187, 2007.
  26. Chen, D. and H. Chen, "Highly birefringent low-loss terahertz waveguide: Elliptical polymer tube," *Journal of Electromagnetic Waves and Applications*, Vol. 24, No. 11–12, 1553–1562, 2010.
  27. Wu, J.-J., D. Chen, K.-L. Liao, T.-J. Yang, and W.-L. Ouyang, "The optical properties of Bragg fiber with a fiber core of 2-dimension elliptical-hole photonic crystal structure," *Progress In Electromagnetics Research Letters*, Vol. 10, 87–95, 2009.
  28. Chau, Y.-F., C.-Y. Liu, H.-H. Yeh, and D. P. Tsai, "A comparative study of high birefringence and low confinement loss photonic crystal fiber employing elliptical air holes in fiber cladding with tetragonal lattice," *Progress In Electromagnetics Research B*, Vol. 22, 39–52, 2010.

29. Chen, D., M.-L. V. Tse, and H. Y. Tam, "Optical properties of photonic crystal fibers with a fiber core of arrays of subwavelength circular air holes: birefringence and dispersion," *Progress In Electromagnetics Research*, Vol. 105, 193–212, 2010.
30. Ferrando, A., E. Silvestre, P. Andres, J. Miret, and M. Andres, "Designing the properties of dispersion-flattened photonic crystal fibers," *Opt. Express*, Vol. 9, 687–697, 2001.
31. Huttunen, A. and P. Törmä, "Optimization of dual-core and microstructure fiber geometries for dispersion compensation and large mode area," *Opt. Express*, Vol. 13, 627–635, 2005.
32. Nozhat, N. and N. Granpayeh, "Specialty fibers designed by photonic crystals," *Progress In Electromagnetics Research*, Vol. 99, 225–244, 2009.
33. Agrawal, A., N. Kejalakshmy, J. Chen, B. M. A. Rahman, and K. T. V. Grattan, "Golden spiral photonic crystal fiber: Polarization and dispersion properties," *Opt. Lett.*, Vol. 33, 2716–2718, 2008.
34. Agrawal, A., N. Kejalakshmy, B. M. A. Rahman, and K. T. V. Grattan, "Polarization and dispersion properties of elliptical hole golden spiral photonic crystal fiber," *Appl. Phys. B*, Vol. 99, 717–726, 2010.
35. Folkenberg, J. R., M. D. Nielsen, and C. Jakobsen, "Broadband single-polarization photonic crystal fiber," *Opt. Lett.*, Vol. 30, 1446–1448, 2005.
36. Zhang, F., M. Zhang, X. Liu, and P. Ye, "Design of wideband single-polarization single-mode photonic crystal fiber," *J. Lightwave Technol.*, Vol. 25, 1184–1189, 2007.
37. Lin, A., Z. Zheng, Z. Li, T. Zhou, and J. Cheng, "Ultra-wideband single-polarization single-mode, high nonlinearity photonic crystal fiber," *Opt. Communications*, Vol. 241, 339–348, 2009.
38. Knight, J. C. and D. V. Skryabin, "Nonlinear waveguide optics and photonic crystal fibers," *Opt. Express*, Vol. 15, 15365–15376, 2007.
39. Mortensen, N. A., M. D. Nielsen, J. R. Folkenberg, A. Petersson, and H. R. Simonsen, "Improved large-mode-area endlessly single-mode photonic crystal fibers," *Opt. Lett.*, Vol. 28, 393–395, 2003.
40. Limpert, J., T. Schreiber, S. Nolte, H. Zellmer, T. Tunnermann, R. Iliew, F. Lederer, J. Broeng, G. Vienne, A. Petersson, and C. Jakobsen, "High-power air-clad large-mode-area photonic crystal fiber laser," *Opt. Express*, Vol. 11, 818–823, 2003.
41. Li, J., J. Wang, and F. Jing, "Improvement of coiling mode to

- suppress higher-order-modes by considering mode coupling for large-mode-area fiber laser,” *Journal of Electromagnetic Waves and Applications*, Vol. 24, No. 8–9, 1113–1124, 2010.
42. Saitoh, K. and M. Koshiba, “Full-vectorial imaginary-distance beam propagation method based on finite element scheme: Application to photonic crystal fibers,” *IEEE J. Quantum Electron.*, Vol. 38, 927–933, 2002.
  43. Wu, C., B. O. Guan, Z. Wang, and X. Feng, “Characterization of pressure response of Bragg gratings in grapefruit microstructured fibers,” *J. Lightwave Technol.*, Vol. 28, 1392–1397, 2010.